Synchronous Vibration and Low-Frequency Nonlinear Disturbance Suppression Based on QR-ADRC in Active Magnetic Bearing System

Tianci SUN*, Hongbo SUN*, Feng HU*, Dong JIANG*, Zicheng LIU*

* College of Electrical Engineering, Huazhong University of Science and Technology, Wuhan 430074, Hubei Province,China
Email: jiangd@hust.edu.cn

Abstract

In the magnetic bearing-fluid mechanical loads, surge is a common nonlinear low-frequency vibration under abnormal working conditions. Magnetic bearing motors can also experience same frequency vibration during rotation due to rotor imbalance. These vibrations can cause problems such as noise, collision, and even instability. Active Disturbance Rejection Control (ADRC) can be applied to the suspension control of magnetic levitation systems due to its robustness advantage. This article proposes an active disturbance rejection strategy for magnetic bearings based on quasi-resonant extended state observer (QR-ESO), which can simultaneously suppress both same frequency and low-frequency disturbances of magnetic bearings. Traditional ESO cannot effectively observe the sinusoidal disturbance of rotational frequency caused by rotor unbalance centrifugal force. Therefore, QR-ESO was applied to ADRC for interference estimation, and its sinusoidal disturbance estimation characteristics were analyzed. This study was tested on a 5-axis AMB test bench rotating in 3300 rpm. Centrifugal force disturbances are caused by rotation, and low-frequency currents are injected to simulate large nonlinear disturbances. Compared to traditional PID controllers, the same frequency vibration was attenuated by 26 dB, and the low-frequency vibration was attenuated by 15 dB, demonstrating the effectiveness of the proposed vibration reduction strategy.

Keywords : Active Magnetic Bearing(AMB), Active Disturbance Rejection Control(ADRC), quasi-resonant extended state observer(QR-ESO), vibration suppression

1. Introduction

1.1 Active Magnetic Bearing (AMB)

Active Magnetic Bearings (AMBs) are non-contact bearing devices that utilize magnetic forces to levitate rotors within the air gap, achieving contact-free operation relative to the stator (Maslen & Schweitzer, 2009). Owing to their wear-free operation, lubrication-free design, and zero-contact characteristics, AMBs have been widely implemented in high-speed rotating machinery, particularly in turbomachinery applications such as compressors, where they significantly enhance operational performance. However, vibration remains a critical challenge in rotating machinery, potentially inducing acoustic noise, rotor-stator collisions, and mechanical failures. This paper systematically investigates vibration phenomena in AMB systems.

1.2 Vibration in AMB

The vibration problems faced by magnetic bearings applied in high-speed rotating machinery cover a relatively wide frequency range, mainly including synchronous vibration with the same frequency as the rotational speed and nonlinear low-frequency disturbances caused by sudden changes in fluid pressure. Synchronous vibration is mainly caused by rotor imbalance, and its characteristic frequency is equal to the rotational frequency, which will cause obvious fluctuations in the rotor displacement of the magnetic bearing. Surge is a vibration under abnormal operating conditions that occurs when the flow rate of a turbo-compressor decreases to a certain extent. This low-frequency and high-amplitude air flow oscillation is a large source of exciting force, which will have a greater impact on the axial direction of the magnetic bearing. However, methods that can simultaneously achieve synchronous vibration and low-frequency nonlinear large disturbance suppression are rarer.

For the vibration suppression of synchronous components, Yoon et al. proposed an output regulation method for imbalance compensation in the AMB system (Yoon, 2016). Yutaka et al. analyzed the imbalance effect in the gyroscope sensor and used an imbalance torque estimator for imbalance compensation (Yutaka, 2009). Zheng Yangbo et al. proposed a model-free control (MFC) method based on the Newton-type ILC algorithm to suppress vibration (Zheng, 2019).Cai Kevin et al. applied a zero-phase odd-harmonic repetitive controller to the harmonic suppression of a magnetically levitated centrifugal compressor (Cai, 2020). Sun Hongbo used a generalized integral-frequency-locked loop to extract the rotational speed information from the current signal and designed a compensation link based on the phase-shifted generalized integral for displacement vibration suppression (Sun, 2021). Xu Hongwei proposed a rotor frequency estimator based on a phase-locked loop (PLL) and an imbalance compensator based on coordinate transformation (CT) for displacement vibration suppression (Xu, 2024).

For the surge suppression of low-frequency components, many scholars have conducted research at the compressor body level. Dong Tianlu avoided surge by real-time calculating the surge rotational speed of the compressor under the current operating condition and controlling the actual rotational speed of the compressor not to be lower than the surge rotational speed, but there are limitations on the range of the rotational speed (Dong, 2009). At the control level, Han Xue et al. effectively suppressed the surge in the MSCC system through an ADRC controller (Han, 2022).

1.3 ADRC in AMB

Active disturbance rejection control (ADRC), proposed by Han Jingqing, was further developed by Gao Zhiqiang who introduced bandwidth parameterization for controller tuning (Gao, 2003)(Han, 2009). Tian Gang analyzed the frequency response of ADRC, demonstrating its robustness to parameter variations (Tian, 2007). The ADRC framework primarily consists of a controller and an extended state observer (ESO). By defining actual disturbances and unknown dynamics or parameters as generalized disturbances, the ESO in ADRC observes these generalized disturbances. After effectively estimating the disturbances, a compensation signal is injected into the control input to suppress them. ADRC relies minimally on the system model and incorporates complex disturbance information such as coupling effects, rotor dynamics, and nonlinearities into its generalized disturbance term, making it uniquely advantageous for vibration suppression in magnetic bearings.

In recent years, ADRC has been applied to AMB systems. For example, Zhu Huangqiu applied ADRC to decoupling control of an AMB system, demonstrating good static and dynamic performance in simulations, but only through numerical validation (Zhu, 2009). Wang Shaoshuai combined BP neural networks with ADRC for decoupling control of a three-degree-of-freedom six-pole permanent magnet mechanism, though vibration suppression was not considered (Wang, 2020). Sun Jianzhong parallelized the QR link in the observer to suppress same frequency disturbances, but did not consider low-frequency disturbances (Sun, 2024). Most existing research on vibration suppression in magnetic bearings focuses on synchronous vibration and harmonic suppression, with minimal work on low-frequency nonlinear large disturbances (such as surge). Research capable of simultaneously suppressing both synchronous and low-frequency nonlinear disturbances remains scarce.

2.Active Magnetic Bearing System with ADRC

2.1 The structure and dynamic equations of AMB

Unlike traditional bearings, the AMB system is an active control system. A radial AMB consists of controller, displacement sensors, amplifiers, and actuators. Its basic principle is as follows: displacement sensors mounted on the stator detect the rotor's radial position; the controller generates current commands via control algorithms based on this position; the amplifier produces actual control currents in the coils; and the actuators levitate the rotor via electromagnetic forces. A radial AMB with x and y degrees of freedom in one radial section is shown in Fig. 1.

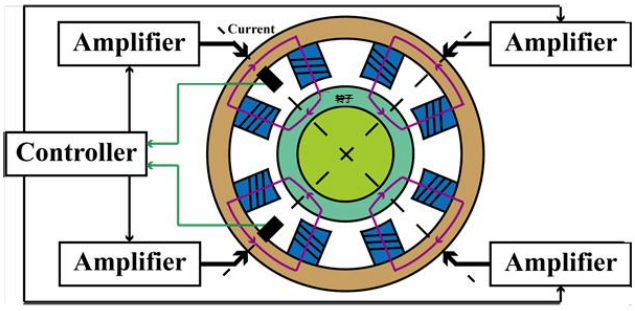

Fig. 1 Structure of radial magnetic bearings

The magnetic force generated by the actuators is a nonlinear function of rotor displacement and coil current. When the rotor displacement is much smaller than the air gap, the magnetic force expression for a pair of actuators at the same degree of freedom can be linearized as equation (1):

$$F = k_i i_c + k_x x_e \tag{1}$$

Here, k_x is the force-displacement stiffness, k_i is the force-current stiffness (both determined by the actuator structure), i_c is the control current, and x_e is the radial displacement. Typically, one degree of freedom is controlled by two opposing windings with differential currents, where i_c represents the current difference.

In a five-axis AMB system practical control, the coupling between axial and radial degrees of freedom is negligible, allowing approximate decoupling. Thus, the dynamic model focuses only on the four radial degrees of freedom. The rotor position is expressed as displacements detected by radial sensors: $q_{se}=[x_{seA}\ x_{seB}\ y_{seA}\ y_{seB}]^{\mathrm{T}}$. To implement active disturbance rejection, taking x_{seB} as an example, the generalized disturbance is defined as:

$$\begin{aligned} f_{xB} = {} & \frac{l_c - l_d}{m l_c}\left[\frac{m l_d}{l_c - l_d}\ddot{x}_{seA} + \frac{l_a k_{xA} + l_b k_{xB} - l_d(k_{xA} + k_{xB})}{l_c - l_d} x_{seA}\right] + \\ & \frac{l_c - l_d}{m l_c}\left[k_{iA} i_{cA} + \frac{l_c(k_{xA} + k_{xB}) - (l_a k_{xA} + l_b k_{xB})}{l_c - l_d} x_{seB} + f_{uxB}\right] + \left(\frac{k_{iB}(l_c - l_d)}{m l_c} - b_0\right) i_{cxB} \end{aligned} \tag{2}$$

The generalized disturbance f_{xB} encompasses actual disturbances, coupling effects with other degrees of freedom, unknown internal dynamics, parameter variations, etc., collectively termed the total disturbance. This total disturbance reduces the controller's reliance on an exact model of the control target. If the total disturbance can be estimated and compensated in the control loop, disturbance suppression can be achieved.

Based on this definition, the dynamic equation for the x_{seB} degree of freedom in the AMB system can be written as:

$$\ddot{x}_{seB} = f_{xB} + b_0 i_{cB} \tag{3}$$

2.2 Analysis of ADRC Based on ESO

To suppress interference, the control current can be designed as:

$$i_{cB} = \frac{-f + i}{b_0} \tag{4}$$

Using this form of control current, the system can be transformed into a second-order integrator controlled by i and disturbed by f_{xB}. An observer is established to estimate f_{xB}, where $X = \begin{bmatrix} \dot{x}_{seB} & x_{seB} & f_{xB} \end{bmatrix}^T$ is the state variable and $y=[x_{seB}]$ is the output variable. Since the state variable X includes the generalized disturbance f_{xB}, X is called the extended state. According to control theory, an Extended State Observer (ESO) can be constructed to estimate the state variables, and its state-space representation in the z-domain is:

$$\begin{aligned} \dot{Z} &= AZ + Bi_{cB} + L(y - \hat{y}) \\ \hat{y} &= CZ \end{aligned} \tag{5}$$

Where $L=[l_1\ l_2\ l_3]^{\mathrm{T}}$, and L is a parameter vector affecting the stability and convergence of the observer.

The z_3 term in ESO is an estimate of the total disturbance f_{xB}. Therefore, subtracting the z_3 term from the control current i_{cB} can suppress vibration. When ESO works effectively, a PD controller is used according to the estimated displacement and its derivative. Once the total disturbance is estimated, generating a reverse compensation current in the control current can suppress the disturbance.

In the observer observation, the transfer function from the generalized disturbance f_{xB} to the disturbance estimation error r_3 can be calculated according to equation (6):

$$H_{r3} = \frac{r_3(s)}{f_{xB}(s)} = \frac{s(s^2 + 3\omega_0 s + 3\omega_0^2)}{(s + \omega_0)^3} \tag{6}$$

Where ω_0 is the bandwidth of the observer for observing disturbances. Generally, the bandwidth of the observer is larger than that of the controller. According to the amplitude-frequency characteristic of H_{r3}, in the low-frequency band, the gain of the estimation error is small, so ESO can estimate the interference when the interference frequency is low. Increasing ω_0 can reduce the estimation error. However, ω_0 is limited by noise. If ω_0 is too large, the anti-interference ability will decrease.

However, if the rotation frequency is set to 100Hz-500Hz, synchronous disturbances cannot be effectively observed. Therefore, under the action of rotor centrifugal force, the displacement generally produces an elliptical motion trajectory, unable to accurately levitate at the center of the air gap, and there will still be synchronous disturbance components,

making it impossible to accurately and advanced control the rotor. Therefore, QR-ESO is proposed to observe and suppress synchronous disturbances.

3. The Principle of QR-ESO and Its Stability Proof

3.1 Structure of QR-ESO

Compared with the ordinary integrator *1/s*, quasi-resonant extended state observer (QR-ESO) has a larger gain at $s=j\omega_r$ and adds a quasi-resonant link. Therefore, ordinary integrators can be used to observe DC-type or low-frequency disturbances, while QR-ESO can be used to observe disturbances at the rotation frequency ω_r. The AMB control system of active disturbance rejection control based on third-order QR-ESO is shown in Figure 2. Compared with ESO, QR-ESO has a quasi-resonant part parallel to the integrator for observing synchronous disturbances.

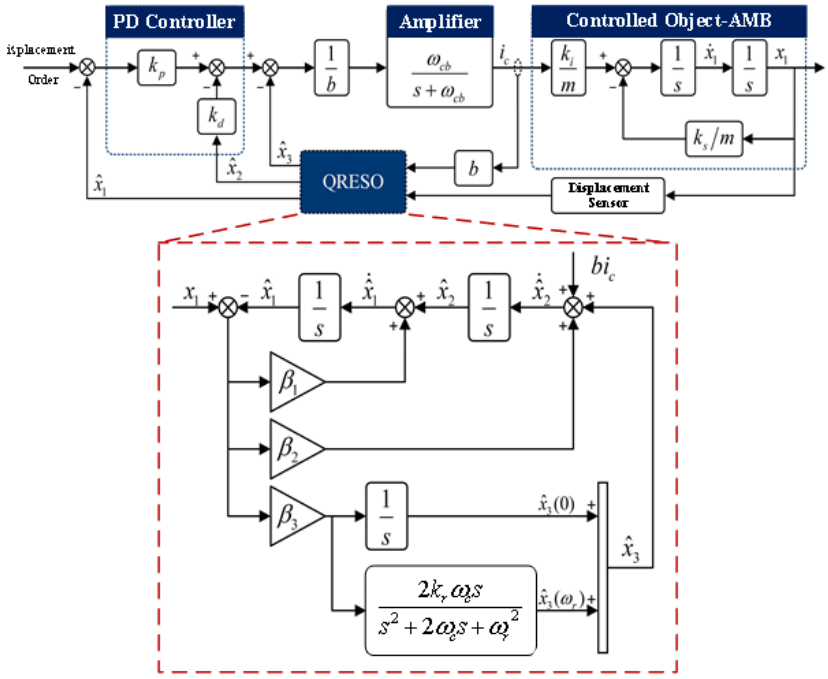

Fig. 2 Structure of AMB system based on QR-ESO for Active Disturbance Rejection Control

The main difference between QR-ESO and ESO lies in the transfer function of z_3 :

$$\dot{z}_3 = l_3(y-\hat{y})(1+sT(s)) \tag{7}$$

The transfer function from the disturbance f_{xB} to the QR-ESO estimation error z_3 is:

$$H_{gr3}(s)=\frac{r_3(s)}{f_{xB}(s)}=\frac{s(s^2+3\omega_0 s+3\omega_0^2)}{(s+\omega_0)^3+s\omega_0^3 T(s)} \tag{8}$$

Compared with ordinary ESO, QR-ESO has three additional parameters. ω_r is the resonant frequency of the observer, usually selected as the rotation frequency. k_r is the quasi-resonant gain, which needs to be set to an appropriate size to observe synchronous disturbances, but excessive k_r will lead to instability. ω_c is the notch bandwidth at the resonant frequency point. Figure 3 is the Bode diagram of the transfer function from the disturbance f_{xB} to the estimation error z_3:

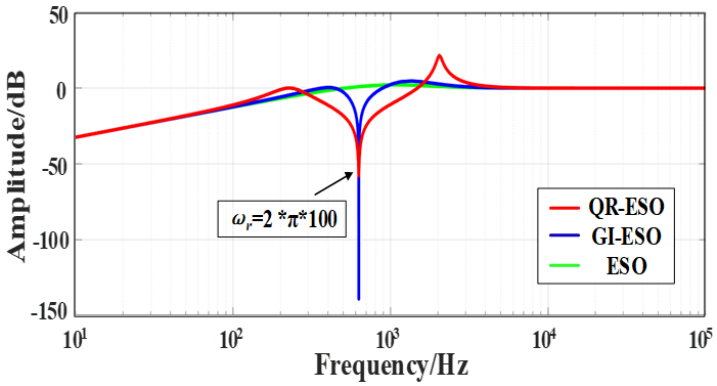

Fig. 3 Bode figure of H_{gr3} with QR-ESO

QR-ESO has notch filtering characteristics at the resonant frequency point $s=j\omega_r$. When QR-ESO is used to observe disturbances with a frequency of ω_r , the estimation error will converge to zero. The Bode diagram of GI-ESO is listed in Figure 3 for comparison. It can be seen that GI-ESO has a larger attenuation gain at the resonant frequency point but a smaller resonant bandwidth. Compared with QR-ESO, GI-ESO has lower tolerance to rotation frequency observation errors. If the observed rotation frequency deviates from the actual motor rotation frequency, GI-ESO has poor observation effect on synchronous disturbances.

3.2 Stability Analysis of QR-ADRC

To analyze the stability of the system, the equivalent structure of the AMB system is derived using the control strategy based on QR-ADRC. It is assumed that the control system applying QR-ADRC is equivalent to the structure shown in Figure 5 of Section 3.2.

According to Newton's law and the linearized formula of the electromagnetic force of the magnetic bearing, for a single degree of freedom:

$$\dot{x}_1 = \frac{k_i}{ms} i_c - \frac{k_s}{ms} x_1 z \tag{9}$$

If the power amplifier is equivalent to an ideal model, the control current i_c can be expressed as:

$$i_c = -\frac{\omega_{cb}/b}{s+\omega_{cb}}(k_p\hat{x}_1 + k_d\hat{x}_2 + \hat{x}_3) \tag{10}$$

Taking the control current i_c , displacement, first-order derivative of displacement, observed displacement, and its derivatives as state variables, the system is analyzed using the state-space method. The state equation of the system can be expressed as:

$$X_{(k+1)} = G \cdot X_{(k)} \tag{11}$$

Where

$$X_{(k+1)} = \left[i_c \quad \dot{x}_1 \quad x_1 \quad \hat{x}_1 \quad \hat{x}_2 \quad \hat{x}_3(0) \quad z_1 \quad z_2 \right]^T_{(k+1)}$$

$$X_{(k)} = \left[i_c \quad \dot{x}_1 \quad x_1 \quad \hat{x}_1 \quad \hat{x}_2 \quad \hat{x}_3(0) \quad z_1 \quad z_2 \right]^T_{(k)}$$

Where X is the state variable selected by the control system. G is the control matrix of the entire system, representing the iterative relationships between the selected state variables.

The system matrix G have only negative real parts, that is, they are within the unit circle on the z-plane, the system is stable. To analyze the stability of the system, parameters are tuned. Taking the quasi-resonant gain ω_r parameter of QR-ESO as an example, the stability of the system is explained. Other parameters are set according to the parameters of the actual system. The root locus changes of the system are shown in Figure 4.

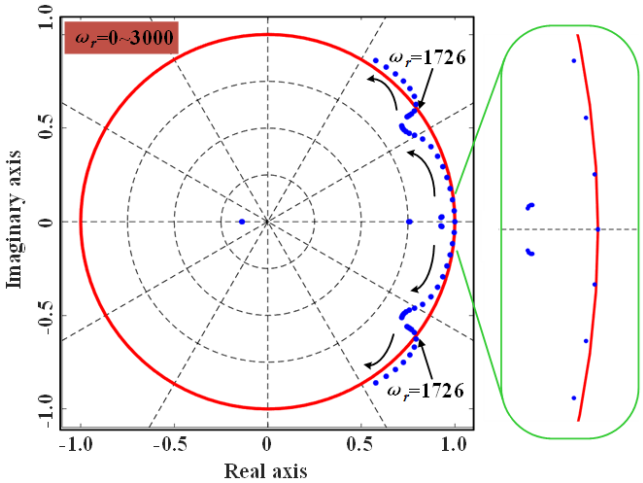

Fig. 4 Root locus of magnetic bearing system in different ωr

According to the derived form of the G matrix, the characteristic polynomial of the system has eight characteristic roots. It can be seen from the root locus diagram that when the rotation frequency $\omega_r/2\pi$ is lower than 1726Hz, all characteristic roots are located within the unit circle, and the system remains stable. Therefore, below the rotation frequency of 1726Hz, QR-ADRC can achieve stable control and can be used to suppress the vibration of the system. The stable rotation frequency range is large enough for the normal operation of the AMB system. Other parameters of the

magnetic bearing system can also be designed using this method.

4.Experimental Results

Table 1 Experimental Parameter Settings

Parameter	Value
Motor Rated Power P	200 kW
Rated Rotation Speed	18000 rpm
Experimental Rotation Speed	3300 rpm
Switching/Sampling Frequency	
Force-Displacement Stiffness k_x	$2.4*10^6$ N/m
Force-Current Stiffness k_i	129.7 N/A
ESO Bandwidth $\omega_0/2\pi$	200 Hz
PD Controller Bandwidth $\omega_{c0}/2\pi$	150 Hz
Quasi-Resonant Frequency $\omega_r/2\pi$	65 Hz
Quasi-Resonant Gain k_r	10
Quasi-Resonant Bandwidth ω_c	1 Hz

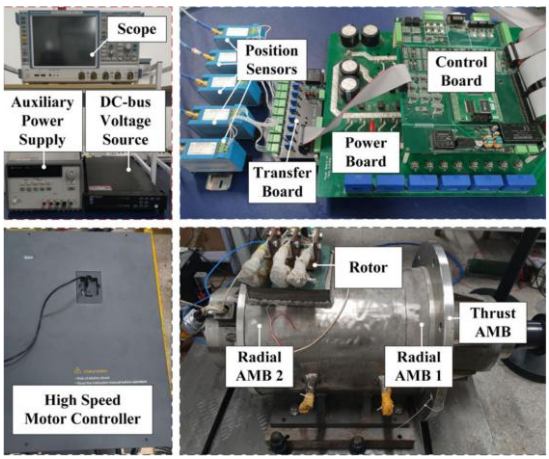

Fig. 5 Structure of the magnetic bearing experimental platform

An AMB test rig was established to validate the proposed control strategy. The test rig consists of two radial magnetic bearings, one axial magnetic bearing, two protective contact bearings, a high-speed motor, and a power board. Figure.5 shows the layout and structural schematic of the test rig. The amplifier is composed of an IGBT circuit with an H-half-bridge topology and a switching frequency of 20 kHz. Eddy current sensors are used to detect rotor displacement. The control process is as follows: in each switching cycle, the displacement sensor measures the displacement of each degree of freedom and converts it into an electrical signal. The controller generates PWM signals and displacement signals based on the control algorithm to drive the amplifier, which produces the actual current through the PWM signals and IGBT circuit to levitate the rotor.

The air gap of the magnetic bearing is ±500 μm, and the protective bearing air gap is ±250 μm. When levitated, the rotor is centered in the protective bearing air gap in all five degrees of freedom, with maximum displacement fluctuations not exceeding 5 μm. After levitation, the rotor is driven to rotate by a high-speed motor at 3300 rpm. Rotor imbalance generates synchronous sinusoidal disturbances in the magnetic bearings during rotation. In this study, a sinusoidal interference signal with a frequency of 5 Hz and amplitude of 0.2 A is injected into the z-axis control current to simulate low-frequency nonlinear large disturbances.

To obtain information about the position loop, the frequency characteristics of the controller were investigated by sweeping the frequency response under three control methods on the experimental platform.

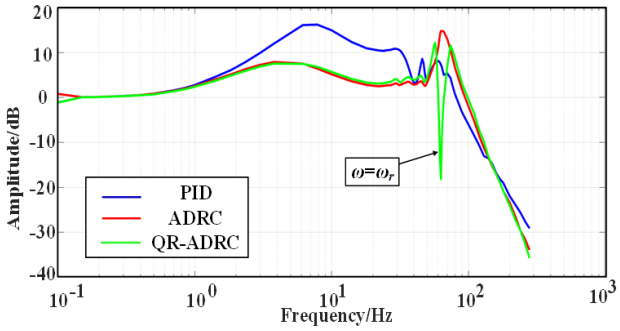

Fig. 6 Frequency sweep results of closed-loop transfer function of different controllers

The frequency sweep results in Fig. 6 show that both the ordinary ADRC control and the proposed QR-ADRC control exhibit significantly reduced amplitude gains in the low-frequency band (5 Hz to 40 Hz) compared to PID control, with an attenuation effect exceeding 10 dB, effectively suppressing low-frequency disturbances. Due to the QR link, QR-ADRC has a significantly lower gain at the resonant frequency than ordinary ADRC, enabling suppression of synchronous disturbances. This is consistent with theoretical analysis, simulations, and experimental results. The frequency sweep results visually demonstrate the optimization of the proposed control method on the overall system control performance.

As shown in Fig. 7, under PID control, the rotor displacement exhibits large fluctuations containing both low-frequency and synchronous vibration components. Switching first to ordinary ADRC control and then to QR-ADRC

control, the peak-to-peak fluctuation amplitude decreases from 210 μm under PID control to 100 μm under ADRC control and further to 30 μm under QR-ADRC control. After switching from PID to ADRC control, low-frequency disturbances

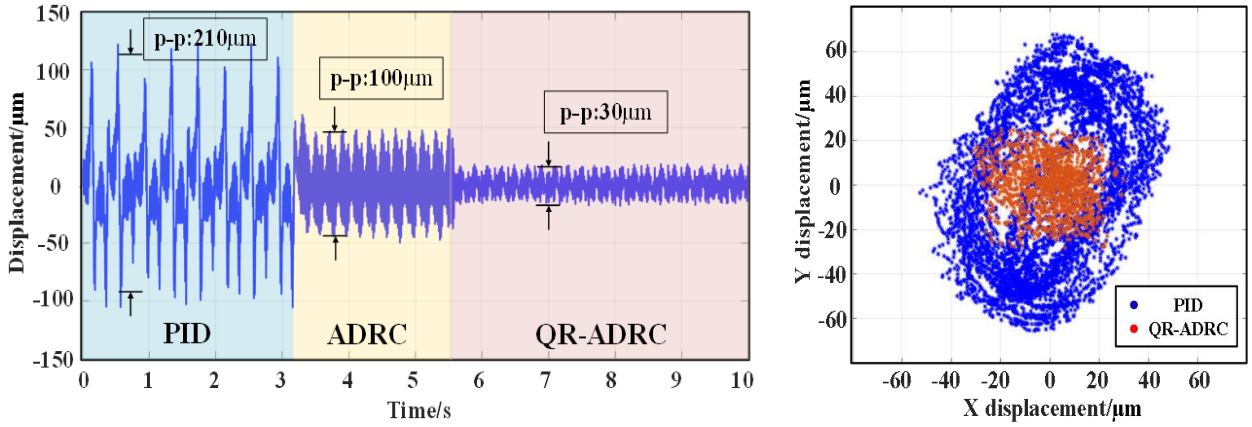

Fig. 7 Displacement Vibration Suppression Time Domain Results in x-axis and in x-y plane diagram

are well suppressed, but due to the lack of synchronous disturbance observation, rotor centrifugal force still causes significant vibrations.

The x-y plane diagram in Fig. 7 also shows that displacement vibrations are effectively suppressed using the QR-ADRC algorithm, with the rotor levitated at the center of the protective bearing air gap and significantly reduced fluctuations.

The rotor displacement spectrum is shown in Fig. 8.

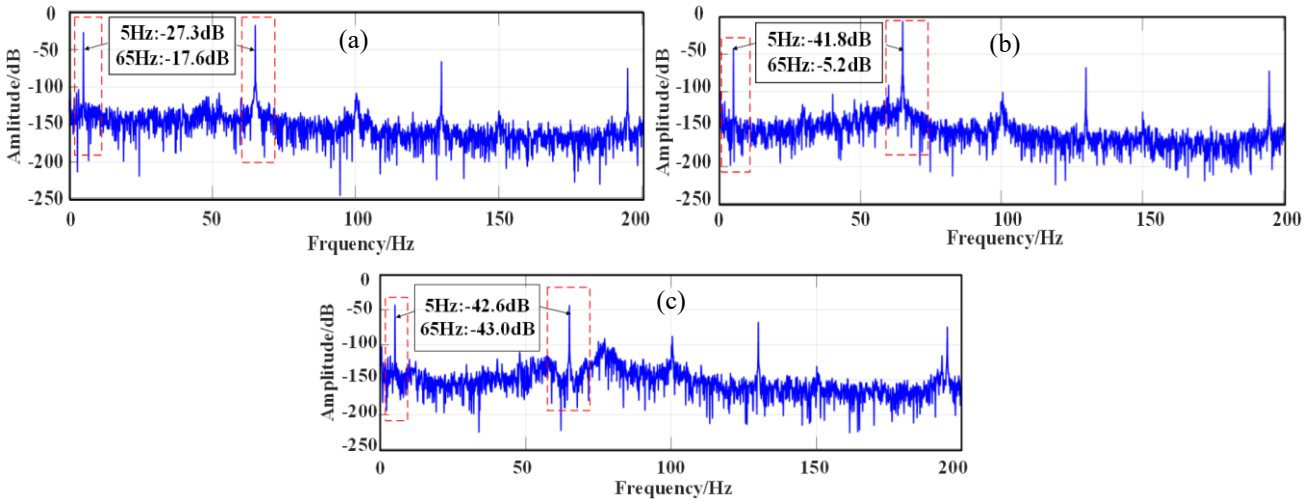

Fig. 8 Frequency domain results of displacement vibration suppression (a) PID (b) ADRC (c) QR-ADRC

After replacing ESO with QR-ESO, rotor displacement fluctuations are further reduced. The spectrum amplitude is plotted with a reference of 50. Compared to the traditional PID controller, the synchronous vibration at 65 Hz decreases from -17.6 dB to -43.0 dB (26 dB attenuation), and the low-frequency vibration at 5 Hz decreases from -27.3 dB to -42.6 dB (26 dB attenuation), both effectively suppressed. The time-domain and frequency-domain results confirm the effectiveness of the vibration suppression strategy and demonstrate that QR-ADRC can be effectively applied in AMB.

5. Conclusions

This paper analyzes vibration suppression in magnetic bearings and proposes a vibration reduction strategy based on a QR-ADRC, achieving simultaneous suppression of low-frequency nonlinear disturbances and rotor unbalance disturbances in magnetic levitation bearings for rotating machinery supports.

First, the principle of active disturbance rejection control for magnetic bearings was designed and analyzed. The limitations of ESO in observing sinusoidal disturbances were discussed, followed by the design and analysis of an active disturbance rejection controller based on QR-ESO. Frequency-domain analysis shows that QR-ESO outperforms ESO in suppressing sinusoidal disturbances.

Experimental results indicate that the ADRC controller with QR-ESO achieves excellent levitation control. The adaptive active disturbance rejection controller effectively suppresses vibrations in the levitation system, verifying the

effectiveness of QR-ADRC in addressing both synchronous and low-frequency vibrations in magnetic levitation systems. Due to the strong robustness of the active disturbance rejection controller, parameters designed using an approximate model can still be applied in experiments, simplifying parameter design for practical applications.

Thanks

We sincerely thank all the teachers in Jiang Dong's research group and our students for their meticulous and patient guidance. We would like to express our gratitude to all senior and junior colleagues in the research group for their support and valuable discussions. Finally, we would like to express our gratitude to our predecessors for their outstanding contributions in the field of ADRC. Their fruitful research has provided valuable insights and references for our work.

References

B. Guo, S. Bacha, M. Alamir, A. Hably and C. Boudinet, "Generalized Integrator-Extended State Observer With Applications to Grid-Connected Converters in the Presence of Disturbances," in IEEE Transactions on Control Systems Technology, vol. 29, no. 2, pp. 744-755, March 2021, doi: 10.1109/TCST.2020.2981571.

Cai, K., Deng, Z., Peng, C., & Li, K. "Suppression of Harmonic Vibration in Magnetically Suspended Centrifugal Compressor Using Zero-Phase Odd-Harmonic Repetitive Controller," in *IEEE Transactions on Industrial Electronics*, vol. 67, no. 9, pp. 7789-7797, Sept. 2020, doi: 10.1109/TIE.2019.2942574.

Dong, T. *Centrifugal/Screw Refrigeration Units and Applications* [M]. Beijing: China Machine Press, 2001. (in Chinese).

Gao, Z. "Scaling and bandwidth-parameterization based controller tuning," *Proceedings of the 2003 American Control Conference*, 2003., Denver, CO, USA, 2003, pp. 4989-4996, doi: 10.1109/ACC.2003.1242516.

Han, J. "From PID to Active Disturbance Rejection Control," in *IEEE Transactions on Industrial Electronics*, vol. 56, no. 3, pp. 900-906, March 2009, doi: 10.1109/TIE.2008.2011621.

Han, X., Liu, G., Chen, B., & Zheng, S. "Surge Disturbance Suppression of AMB-Rotor Systems in Magnetically Suspension Centrifugal Compressors," in *IEEE Transactions on Control Systems Technology*, vol. 30, no. 4, pp. 1550-1560, July 2022, doi: 10.1109/TCST.2021.3112765.

Maruyama, Y., Mizuno, T., Takasaki, M., et al. "Application of Rotor Unbalance Compensation to an AMB-Based Gyroscopic Sensor," *Journal of System Design & Dynamics*, 2009, 3(4):572-583.

Schweitzer, G., & Maslen, E. H. *Magnetic bearings: theory, design, and application to rotating machinery* [M]// *Magnetic Bearings—Theory, Design and Application to Rotating Machinery*. 2009.

Sun, H. *Research on Vibration Suppression of Active Magnetic Bearing System* [D]. Wuhan: Huazhong University of Science and Technology, 2021. (in Chinese).

Sun, J. Z., Song, W. H., Fan, P. H., et al. (2024). Modeling of active magnetic bearing system and vibration suppression via quasi-resonant active disturbance rejection control. Journal of Vibration and Shock, *43*(13), 227–236+287.

Tian, G., & Gao, Z. "Frequency Response Analysis of Active Disturbance Rejection Based Control System," 2007 *IEEE International Conference on Control Applications*, Singapore, 2007, pp. 1595-1599, doi: 10.1109/CCA.2007.4389465.

Wang, S., Zhu, H., Wu, M., & Zhang, W. "Active Disturbance Rejection Decoupling Control for Three-Degree-of-Freedom Six-Pole Active Magnetic Bearing Based on BP Neural Network," in *IEEE Transactions on Applied Superconductivity*, vol. 30, no. 4, pp. 1-5, June 2020, Art no. 3603505, doi: 10.1109/TASC.2020.2990794.

Xu, H., Li, J., Lu, Y., & Li, H. "Unbalance Control for High-Speed Active Magnetic Bearing Systems Without Speed Sensors," in *IEEE Transactions on Transportation Electrification*, doi: 10.1109/TTE.2024.3366551.

Yang, X., Hu, H., Liu, Y., & He, Z. "A Quasi-Resonant Extended State Observer-Based Predictive Current Control Strategy for Three-Phase PWM Rectifier," in *IEEE Transactions on Industrial Electronics*, vol. 69, no. 12, pp. 13910-13917, Dec. 2022, doi: 10.1109/TIE.2021.3137441.

Yoon, S. Y., Di, L., & Lin, Z. "Unbalance compensation for AMB systems with input delay: An output regulation approach," *Control Engineering Practice*, 2016, 46:166-175.

Zheng, Y., Mo, N., Zhou, Y., & Shi, Z. "A Model-Free Control Method for Synchronous Vibration of Active Magnetic Bearing Rotor System," in *IEEE Access*, vol. 7, pp. 79254-79267, 2019, doi: 10.1109/ACCESS.2019.2923358.

Zhu, H. Q., Chen, J. J., & Sun, X. D. "Active disturbances rejection decoupling control for active magnetic bearing multivariable system," *International Journal of Modelling Identification & Control*, 2009, 7(1):119-125.